H₂ Formation on Interstellar Grains and the Fate of Reaction Energy

Stefano Pantaleone[1,6] , Joan Enrique-Romero[1,2] , Cecilia Ceccarelli[1] , Stefano Ferrero[2] , Nadia Balucani[1,3,4] ,
Albert Rimola[2] , and Piero Ugliengo[5]

[1] Université Grenoble Alpes, CNRS, Institut de Planétologie et d'Astrophysique de Grenoble (IPAG), F-38000 Grenoble, France
stefano.pantaleone@univ-grenoble-alpes.fr
[2] Departament de Química, Universitat Autònoma de Barcelona, Bellaterra, E-08193, Catalonia, Spain
[3] Dipartimento di Chimica, Biologia e Biotecnologie, Università di Perugia, Via Elce di Sotto 8, I-06123 Perugia, Italy
[4] Osservatorio Astrofisico di Arcetri, Largo E. Fermi 5, 50125 Firenze, Italy
[5] Dipartimento di Chimica and Nanostructured Interfaces and Surfaces (NIS) Centre, Università degli Studi di Torino, via P. Giuria 7, I-10125, Torino, Italy
Received 2021 March 26; revised 2021 April 27; accepted 2021 May 12; published 2021 August 16

Abstract

Molecular hydrogen is the most abundant molecular species in the universe. While no doubts exist that it is mainly formed on the interstellar dust grain surfaces, many details of this process remain poorly known. In this work, we focus on the fate of the energy released by the H₂ formation on the dust icy mantles: how it is partitioned between the substrate and the newly formed H₂, a process that has a profound impact on the interstellar medium. We carried out state-of-the-art ab initio molecular dynamics simulations of H₂ formation on periodic crystalline and amorphous ice surface models. Our calculations show that up to two-thirds of the energy liberated in the reaction ($\sim$300 kJ mol^{-1} $\sim$3.1 eV) is absorbed by the ice in less than 1 ps. The remaining energy ($\sim$140 kJ mol^{-1} $\sim$1.5 eV) is kept by the newly born H₂. Since it is 10 times larger than the H₂ binding energy on the ice, the new H₂ molecule will eventually be released into the gas phase. The ice water molecules within $\sim$4 Å from the reaction site acquire enough energy, between 3 and 14 kJ mol^{-1} (360–1560 K), to potentially liberate other frozen H₂ and, perhaps, frozen CO molecules. If confirmed, the latter process would solve the long standing conundrum of the presence of gaseous CO in molecular clouds. Finally, the vibrational state of the newly formed H₂ drops from highly excited states ($\nu = 6$) to low ($\nu \leqslant 2$) vibrational levels in a timescale of the order of picoseconds.

Unified Astronomy Thesaurus concepts: Astrochemistry (75)

1. Introduction

Molecular hydrogen is the most abundant molecule in the universe. Its formation is also the first step of the interstellar chemistry and, therefore, a fundamental reaction. In molecular clouds, H₂ is mainly formed via the H + H association reaction on the interstellar dust grain surfaces, which act as a third body capable of partially absorbing the energy ($\sim$440 kJ mol^{-1} $\sim$4.56 eV) released by the chemical reaction and, consequently, stabilize the newly formed H₂ molecule (e.g., van de Hulst 1946; Hollenbach & Salpeter 1970, 1971; Smoluchowski 1983). Although no doubts exist regarding the occurrence of this process, many specific details remain poorly known (see, e.g., Vidali 2013; Wakelam et al. 2017).

Here, we focus on the fate of the energy released by the reaction, which has been a source of debate for decades. Specifically, how much of the reaction energy is absorbed by the dust grain and in what timescale? What fraction of the chemical energy does go into the kinetic energy of the newly formed H₂? Is this energy large enough as H₂ breaks the interaction with the surface and proceeds into the gas phase? How much energy does the H₂ molecule possess when it leaves the grain surface and in what rovibrational state? And, finally, is the energy transmitted to the dust grain enough to locally warm it up and make adjacent frozen molecules sublimate? These points have a profound impact on several aspects of

astrochemistry and, more generally, the physics and chemistry of the interstellar medium (ISM; Duley & Williams 1993).

Answers to the above questions largely depend on the nature of the substrate, namely the specific dust grain surface or, in practice, the interstellar environment where H₂ forms. Here we focus on cold ($\sim$10 K) molecular clouds. In these environments, the grain refractory cores are coated by water-dominated icy mantles either in polycrystalline or amorphous (ASW for amorphous solid water) phases, the latter dominating over the former (Smith et al. 1988; Whittet 1993; Boogert et al. 2015).

Unfortunately, laboratory experiments cannot entirely reproduce the interstellar conditions so that, while they can suggest routes and processes, they cannot provide definitive answers to the above-exposed questions (see, e.g., Vidali 2013). For example, obtaining experimentally how the H₂ formation nascent energy is partitioned is very difficult (Hornekær et al. 2003; Roser et al. 2003; Watanabe et al. 2010; Hama et al. 2012). Computational chemistry methods can be regarded as a complementary tool and, sometimes, as a unique alternative to laboratory experiments. So far, a limited number of studies devoted to the energy dissipation of the H₂ formation reaction on icy grains has appeared in the literature (Takahashi et al. 1999a; Takahashi & Uehara 2001; Herbst & Cuppen 2006).

Here, we present a new theoretical study on the dissipation of the energy released by the H + H → H₂ reaction on water ice using ab initio molecular dynamics simulations (AIMDs). We simulated the reaction adopting a Langmuir–Hinshelwood mechanism (i.e., both reactants are adsorbed on the surface in neighboring sites) both on amorphous and crystalline periodic models of interstellar icy mantles.

[6] Present addresses: Dipartimento di Chimica and Nanostructured Interfaces and Surfaces (NIS) Centre, Università degli Studi di Torino, via P. Giuria 7, I-10125 Torino, Italy and Dipartimento di Chimica, Biologia e Biotecnologie, Università di Perugia, Via Elce di Sotto 8, I-06123 Perugia, Italy.

2. Computational Details

2.1. Methods

All our calculations were carried out with the CP2K package (Hutter et al. 2014). Core electrons were described with the Goedecker–Teter–Hutter pseudopotentials (Goedecker et al. 1996) and valence ones with a mixed Gaussian and plane-wave (GPW) approach (Lippert et al. 1997). The density functional theory (DFT) Perdew–Burke–Ernzerhof (PBE) method was adopted (Perdew et al. 1996), combined with a triple-ζ basis set for valence electrons with a single polarization function (TZVP), and the a posteriori D3 Grimme correction to account for dispersion forces (Grimme et al. 2010, 2011). The plane-wave cutoff was set to 600 Ry. Ice surfaces were thermalized (see Section 2.2), and during the geometry optimization only the reacting H atoms (those forming H_2) were allowed to move, keeping the water molecules fixed at their thermalized positions. All calculations were carried out within the unrestricted formalism as we deal with open-shell systems (see the Appendix for more details). The binding energy (BE) of H_2 was calculated as:

$$BE_{H_2} = E_{CPLX} - (E_{Ice} + E_{H_2}), \qquad (1)$$

where E_{CPLX} is the energy of the H_2/ice system, E_{Ice} is the energy of the bare ice surface, and E_{H_2} is the energy of the H_2 alone.

AIMDs were carried out within the NVE (N = number of particles, V = volume, E = energy) ensemble, where the total energy V_{TOT} (i.e., potential + kinetic) is conserved. The evolution of the system was followed for 5 ps for the crystalline model and for 1 ps for the amorphous model, using time steps of 0.2 fs.
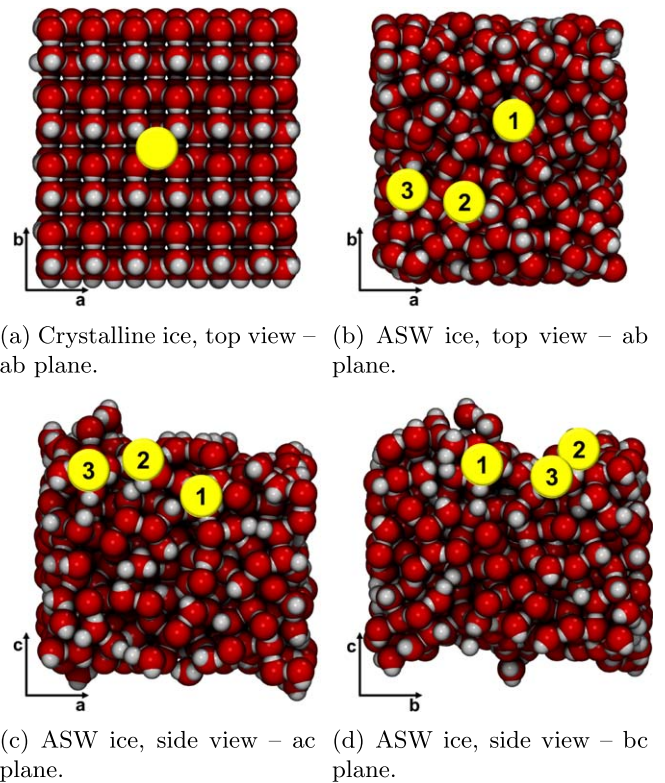
2.2. Ice Models

For the crystalline ice model, a periodic slab cut from the hexagonal ice bulk structure was used. The periodic cell parameters defining the system are $a = 26.318$ Å and $b = 28.330$ Å, while the slab thickness is ~21 Å (corresponding to seven layers), for a total of 576 water molecules. The c parameter of the simulation box, i.e., the nonperiodic one, was set to 50 Å to avoid interactions among the fictitious slab replicas. The size of the slab model was chosen to avoid nonphysical temperature increase due to the extremely large exothermic reaction (Pantaleone et al. 2020).

The amorphous model was obtained by performing a classical molecular dynamics (MD) simulation on the crystalline structure. The MD was carried out with the TIP3P force field (Jorgensen et al. 1983) for 200 ps (with a time step of 0.5 fs) at 300 K within the NVT (N = number of particles, V = volume, T = Temperature) ensemble. A second NVT simulation was performed at 10 K to cool down the system at the temperature of cold molecular clouds. Finally, a geometry optimization and another NVT-MD simulation at 10 K were run using PBE to recover the potential energy surface at the same theory level as described in the previous section.

2.3. H_2 Vibrational State

To calculate the H_2 vibrational state during the AIMDs the anharmonic oscillator model was employed. As a first step, the potential energy surface (PES) of the H_2 isolated molecule was explored by performing a rigid scan of the H–H distance,

(a) Crystalline ice, top view – ab plane.

(b) ASW ice, top view – ab plane.

(c) ASW ice, side view – ac plane.

(d) ASW ice, side view – bc plane.

Figure 1. Top view of the crystalline ice model (a), and top (b) and side ((c) and (d)) views of the ASW ice models. The yellow circles represent the centers of mass of the two H atoms' starting positions. In the case of ASW, the numbers mark the positions (Pos1, Pos2, and Pos3) discussed in the text. The initial H to H distance is about 4 Å (see Figure A1). O atoms are in red and H atoms of the ice are in white.

ranging from 0.3 to 3.0 Å with a step of 0.01 Å. Computed data were fitted with the Morse equation to obtain the force constant of the oscillator, its dissociation energy and, hence, the vibrational levels of H_2. The H_2 turning points calculated with our model were compared with those of the AIMD simulations and the vibrational level was assigned at each H_2 oscillation during the AIMDs.

3. Results

3.1. Reactants Plus Product Positions in the Ice Models

Figure 1 shows the structure of the used crystalline and ASW ice models as well as the starting positions of the center of mass of the two adsorbed H atoms before the reaction. The starting H–H distance, as well as its evolution during the AIMDs is shown in Figure A1. The ASW model presents a rugged morphology (e.g., holes, cavities, and channels) in comparison to the crystalline one and, therefore, we carried out simulations in three positions, roughly representing different possible situations in terms of energetics and surface morphology. The position marked as Pos1 is the deepest one, within a cavity, while positions Pos2 and Pos3 are in the outermost parts of the surface.

As a first step, we optimized the geometries of reactants (the two H atoms) and product (the H_2 molecule) on the water ice surface in order to obtain the potential energy surface of the reaction. No search for transition state structures has been performed because AIMDs indicated this reaction is barrierless at 10 K. That is, the starting kinetic energy of the two H atoms

(a) R - Crystalline (0.0) (b) P - Crystalline (-439.4)

(c) R - ASW (0.0) (d) P - ASW (-436.2)
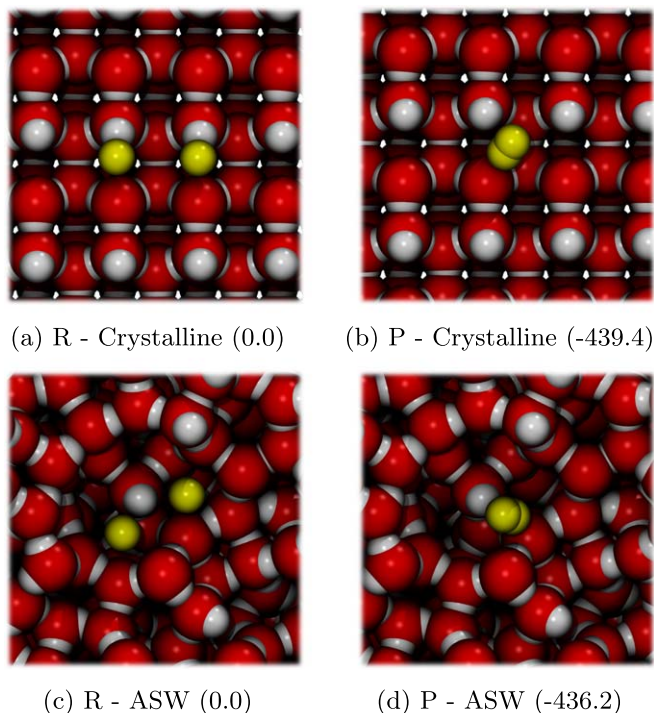
Figure 2. PBE-D3/TZVP optimized geometries of reactants (left panels) and product (right panels) of the H_2 reaction formation on the crystalline (top) and ASW Pos1 (bottom) ice models. The numbers in parentheses correspond to the relative energy in kJ mol^{-1} with respect to the reactants. The H atoms involved in the $H+H \rightarrow H_2$ reaction are in yellow, those belonging to surface water molecules are in white, and O atoms are in red.

Table 1
Results of the AIMD for the H_2 Formation on the Crystalline (First Row) and the ASW Three Position (Figure 1; Bottom Three Rows) Ices

Model	$\frac{K_{ice}}{K_{ice} + K_{H_2}}$	$\frac{K_{H_2}}{K_{ice} + K_{H_2}}$	BE_{H_2} (kJ mol^{-1})	$\nu^{0.2-1}$	ν^{1-5}	E_{peak} (kJ mol^{-1})
Crys.	0.45	0.55	9.0	4–5	1–2	12.0
Pos1	0.65	0.35	9.7	1–2	⋯	43.0
Pos2	0.46	0.54	10.6	6	⋯	7.0
Pos3	0.47	0.53	12.4	5	⋯	7.0

Note. Second and third columns report the fraction of kinetic energy of the ice and the newly formed H_2, respectively, at the end of the simulation (5 and 1 ps for crystalline and ASW ices, respectively). Fourth column reports the H_2 binding energy (in kilojoules per mole) at the reaction site. Fifth and sixth columns report the vibrational state averaged over 0.2–1 ps and 1–5 ps, respectively (the latter can be computed only for the crystalline case). Last column reports the peak energy (in kilojoules per mole) of an ice-molecule neighbor (i.e., at ∼3 Å) to where the reaction occurs.

provided by the 10 K is high enough to overcome the eventually small potential energy barrier. The total energy to be dissipated is around 435–440 kJ mol^{-1}, depending on the surface and starting position.

Figure 2 provides a view of the two H atoms' starting positions and H_2 position immediately after the reaction, on the crystalline and ASW (Pos1 as an example) models, respectively.

3.2. Molecular Hydrogen Desorption

AIMDs results are summarized in Table 1 and shown in Figure 3. First, at least half of the kinetic energy is absorbed by the ice while the remaining one is kept by the newly formed H_2 molecule (∼50%–35%). These numbers are similar for both for the crystalline and ASW ice positions, suggesting they do no depend much on the surface structural details of the ice.

Second, after the H–H bond formation, the newly formed H_2 molecule diffuses over the surface, as it keeps a large kinetic energy, in both crystalline and ASW ice models. However, despite the energetics of the two processes being similar (Figure 3, left panels) the H_2 diffusion (Figure 3, right panels) is different.

On the crystalline surface, the diffusion of the newly formed H_2 over the ice surface is constrained in a specific direction, along the a-axis, parallel to the ice surface, whereas in the b-axis and c-axis directions the starting position does not change. This is because the crystalline model has alternated and opposite electrostatic potentials along the b-axis direction (see Figure A2, which constrains the H_2 diffusion to the perpendicular a-axis, within a channel-like structure created in between the two alternated potential regions (panels (a) and (c)). In

contrast, on the ASW ice model, H_2 diffuses over all three directions, also along the c-axis, which corresponds to direction perpendicular to the ice surface. However, the movement is not the same in the three studied positions. In Pos1, H_2 achieves a maximum height of ∼10 Å over the surface in a timescale of 0.4 ps and does not come back (Figure 3(d)), thus definitely leaving the surface. On the contrary, in Pos2 H_2 slides and hops on the surface within the 1 ps of the simulation (Figure 3(f)). A similar behavior is observed for Pos3, but with wider hops and jumps (Figure 3(h)). This is the key point of the simulations: the kinetic energy remains much larger (∼150 kJ mol^{-1}) than the binding energy (∼10 kJ mol^{-1}) in all cases; therefore, the nascent H_2 is likely doomed to leave the ice surface.

3.3. Energy Dissipation toward the Ice Water Molecules

Figure 4 shows how the energy absorbed by the ice is first transmitted from the reaction site to a neighbor water (i.e., at ∼4 Å) in ∼200–800 fs and, with time, to shells of water molecules with increasing distances. The neighbor water molecule acquires from ∼3 to ∼14 kJ mol^{-1} and stays with that energy for more than about 100–200 fs before the energy is dissipated toward more external water molecules. These timescales are in excellent agreement with previous studies of the sound speed in ices (see, e.g., Ruocco et al. 1996).

3.4. H_2 Vibrational State

The initial state of the H_2 formed on the crystalline ice is $\nu = 4-5$ (obtained averaging over 0.2–1 ps) and then it decreases to $\nu = 1-2$ (1–5 ps average) because of the H_2 energy dissipation. Conversely, at Pos1 of the ASW model, H_2 is formed with a low vibrational state ($\nu = 1-2$, 0.2–1 ps average).

For the other two positions (Pos2 and Pos3), the vibrational state of the newly formed H_2 molecule lies in highly excited states, $\nu = 6$ and $\nu = 5$, respectively. However, our simulations stop at 1 ps and, likely, as on the crystalline ice, the vibrational state of the newly formed H_2 will lower to $\nu = 1-2$. The difference in the behavior between the Pos1 and Pos2/3 is probably due to a transient chemical bond between one of the reacting H and one O atom of a neighboring water molecule (see Figure A3).
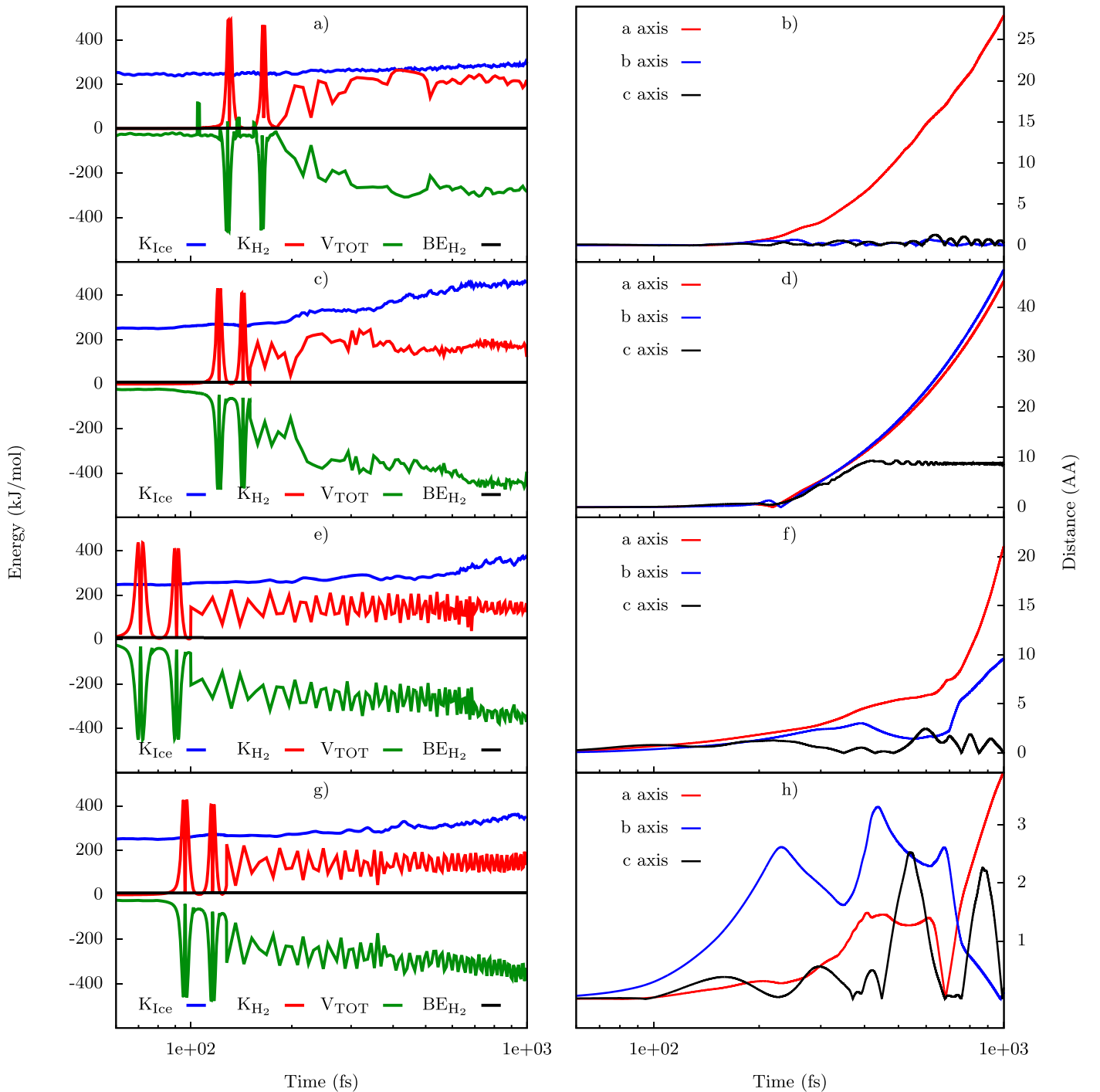
Figure 3. Results of the AIMDs for the crystalline (top panels) and ASW Pos1, Pos2, and Pos3 (panels on the second, third, and bottom rows) models, respectively. Left panels: evolution over time (in fs) of the most relevant energetic components (in kilojoules per mole) of the H_2/ice system for the crystalline (panel (a)) and ASW Pos1, Pos2, and Pos3 (panels (c), (e), and (g)) models, respectively. V_{TOT} is the total potential energy (green lines), K_{H_2} and K_{Ice} are the kinetic energies of H_2 (red lines) and ice (blue lines), respectively, while BE_{H_2} (10 kJ mol^{-1} = 1200 K) is the binding energy of the H_2 (black lines). Right panels: diffusion of the center of mass of the H_2 molecule split into the three Cartesian components—c-axis is the direction perpendicular to the ice surface, while the a- and b-axes are along the ice surface (Section 2).

4. Discussion

4.1. H_2 and Other Molecule Desorption

While there are no doubts that, once formed on the icy surfaces, H_2 molecules will be released into the gas phase, our new computations provide a quantitative and atomistic-view support to this theory. The newly formed H_2 molecules possess an energy much larger than their binding energy, by more than a factor of 10, so that H_2 will very likely be injected into the gas phase. Even in the worst case of crystalline ice, where the simulations show H_2 sliding over the perfect ice surface, the newly formed H_2 will sooner or later stumble onto an imperfection of the ice, and thus its trajectory will be deviated and the molecule will escape into the gas. To have an estimation of the timescale of this phenomenon one could consider the timescale for the newly H_2 to scan the entire
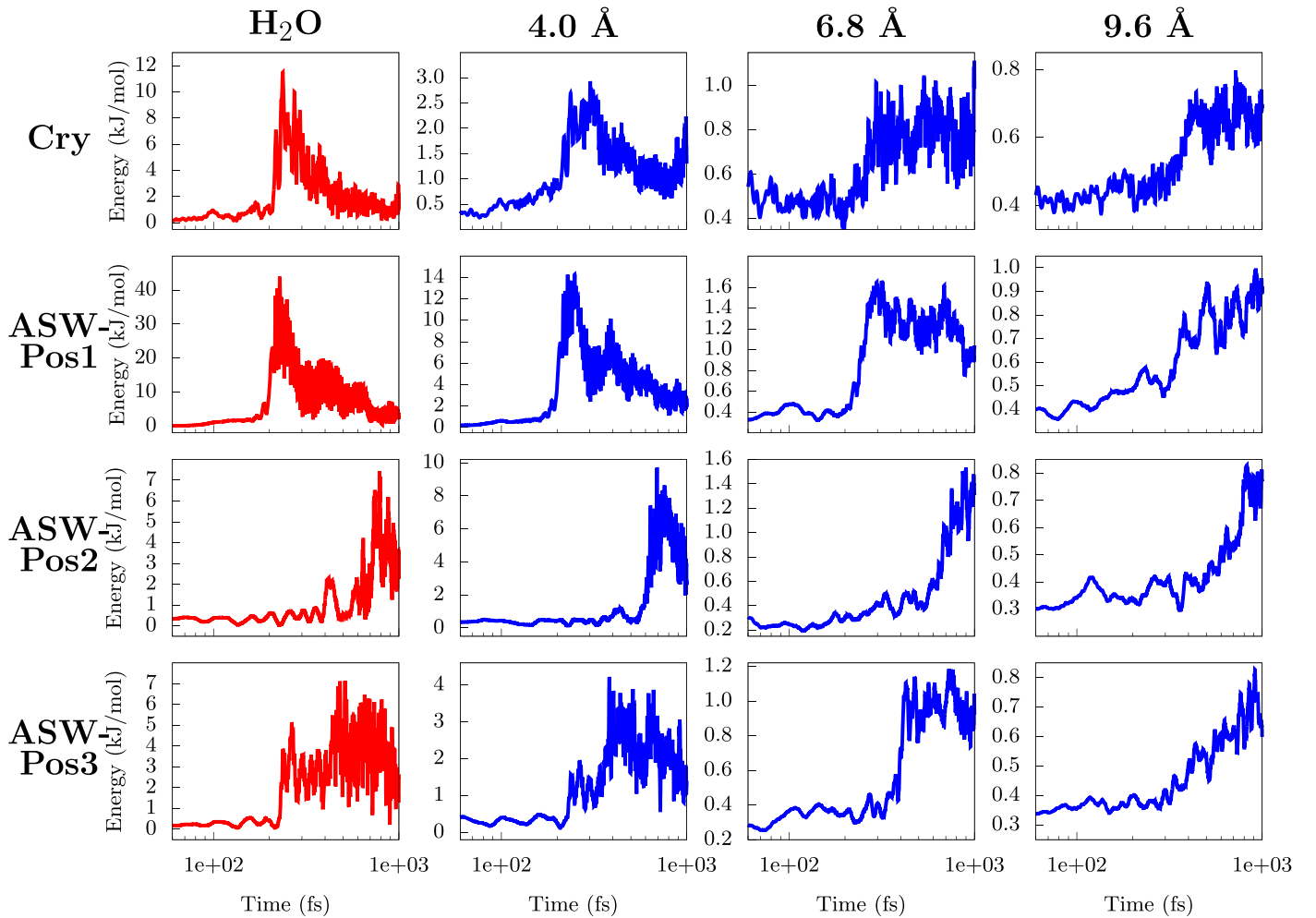
Figure 4. Kinetic energy (in kilojoules per mole) acquired by the water ice molecules as a function of time for the crystalline (top first row panels) and ASW Pos1-3 (lower panels) ices, as marked by the left-hand labels. Left first column panels: energy acquired by a single neighboring water ice molecule (i.e., at ~3 Å) from the H_2 reaction site. Other column panels: energy acquired by the ice surface divided in concentric shells (normalized by the number of water molecules per shell), centered at the reaction site. The labels on the top mark the shells' radii.

surface of an interstellar grain. Assuming its radius is equal to 0.1 μm and each icy site size is equal to 3 Å the number of sites to scan is about 10^5. A first estimate of the time to scan all the sites can be directly obtained by our simulations by considering that about 15 sites of our crystalline ice are covered in less than 1 ps; therefore, to scan the 10^5 it will take less than 10 ns. However, this is strictly true if the H_2 molecule does not loose energy in other minor impacts, so ~10 ns can be considered a lower limit. The upper limit can be computed by assuming that no residual energy is left to the H_2 molecule except the thermal one and, in this case, the velocity to scan is given by the hopping rate and the timescale for scanning the entire grain surface becomes:

$$t_{\mathrm{scan}} = N_s \nu_0^{-1} e^{\frac{E_d}{k_B T_{\mathrm{dust}}}}, \qquad (2)$$

where ν_0 is about 10^{12} s^{-1} and E_d is assumed to be 0.3 times the binding energy (about 400 K). Inserting the numbers, a rough estimate of the time that H_2 takes to leave a typical interstellar grain is $\leqslant 1000$ yr. In laboratory analogs of interstellar grains, the timescale would be even larger, and, consequently, not observable. In conclusion, the newly formed H_2 will leave the surface in a timescale between a few

nanoseconds to a max of about 1000 yr, which is still a very short lifetime with respect to the cloud life.

We want to highlight that the choice of using a proton order ice is just a matter of convenience to test our simulations before going to the more realistic case of the amorphous surface. On a more realistic proton disordered crystalline ice we expect a more anisotropic behavior of the H_2 molecule, and, as a consequence, a faster H_2 desorption.

Our computations also show that the ice absorbs a significant fraction of the reaction energy, 45%–65% (Table 1). This energy propagates like a wave from the point where the H + H reaction occurs (see Figure 4 and also Pantaleone et al. 2020). In ASW ice, a water molecule close to the reaction site acquires 7–43 kJ mol^{-1} (840–5160 K), for more than 100-200 fs. Within the first shell of radius 4 Å, water molecules acquire energies from 3 to 14 kJ mol^{-1} (360–1680 K, average value counting all the water molecules within the first shell). Farther away the energy acquired by the ice-water molecules decreases to less than 1.6 kJ mol^{-1}. The energy acquired by the water ice molecules within a radius of 4 Å from the reaction site could, potentially, be enough to release into the gas phase any molecule whose binding energy is lower than 3–14 kJ mol^{-1}. This could be the case of another H_2 molecule frozen on the ice, a possibility predicted by some astrochemical models (see,

e.g., Hincelin et al. 2015). Indeed, since the binding energy of H_2 is less than $\sim 5 \, kJ \, mol^{-1}$ (e.g., Vidali 2013; Ferrero et al. 2020; Molpeceres & Kästner 2020), several H_2 molecules could be kicked into the gas phase.

More interesting is the case of CO, the most abundant molecule after H_2 in galactic cold molecular clouds. It has a binding energy between 7 and $16 \, kJ \, mol^{-1}$ (e.g., He et al. 2016; Ferrero et al. 2020) so that frozen CO could potentially be liberated into the gas-phase by the formation of H_2. It has been long recognized that, in absence of a nonthermal desorption process, CO in molecular clouds should be entirely frozen onto the interstellar ices in $\sim 3 \times 10^5$ yr (see, e.g., Léger 1983). Several mechanisms have been proposed to explain its presence in the gas (see, e.g., Leger et al. 1985; Schutte & Greenberg 1991; Duley & Williams 1993; Shen et al. 2004; Ivlev et al. 2015). They are all based on the idea that the grain is locally heated and that the frozen molecules are statistically desorbed on a timescale of a few thousands seconds (see, e.g., Hasegawa & Herbst 1993; Herbst & Cuppen 2006), except when faster photodesorption processes are involved. In particular, Duley & Williams (1993) and Takahashi & Williams (2000) focused on the CO desorption caused by the H_2 formation. Using the results of classical MD simulations by Takahashi and colleagues (Takahashi 1999; Takahashi et al. 1999b; Takahashi & Williams 2000) and a statistical approach, these authors found that the surface within a radius of $\sim 4 \, \text{Å}$ from the reaction site is heated up to $\leqslant 40$ K for a time too short (~ 10 fs) to allow CO to sublimate. However, despite the fact that Takahashi's simulations are impressive considering that they were carried out more than 20 yr ago, old force fields (like the TIP3P used by Takahashi et al.) have limitations in describing the actual intermolecular interactions and the energy transfer from one molecule to another, compared to our simulations treated at the quantum mechanical level.

Our AIMDs show that the water molecules within a radius of $4 \, \text{Å}$ from the reaction site can be excited from 3 to $14 \, kJ \, mol^{-1}$ (depending on the position) for more than 100 fs (Figure 4). Using the range of values in the literature for the CO binding energies ($7–16 \, kJ \, mol^{-1}$: He et al. 2016; Ferrero et al. 2020), and the usual Eyring equation to estimate the half-life time of CO desorption, we obtain that a CO molecule within a radius of $4 \, \text{Å}$ from Pos1 would desorb in 33–62 fs, and 69–185 fs from Pos2. On the contrary, CO molecules close to Pos3 and on crystalline ice would not desorb. Therefore, based on this rough argument, the formation of H_2 can potentially desorb frozen CO molecules. Whether this hypothesis is realistic or not depends on (i) how many sites of the AWS ice water molecules are excited as in Pos1 and Pos2, (ii) the ratio of H_2 formation rate with respect to the CO freezing rate ($R = \frac{v(H_2)}{v(CO)}$), and (iii) the probability that CO and H_2 are adjacent.

While a more realistic model for the ASW ice is needed to estimate the first quantity (i), one can estimate the second one (ii) as follows. At steady state, assuming that the $H + H$ reaction has efficiency 1 (e.g., Vidali 2013), the ratio R of the H_2 formation rate with respect to the CO freezing rate is equal to the ratio between the rate of H atoms over CO molecules landing on the grain surface, divided by 2 (because two H atoms are needed for the H_2 formation). Considering an average Milky Way molecular cloud with H_2 density of $10^3–10^4 \, cm^{-3}$, temperature 10 K, a gaseous (undepleted) CO abundance with respect to H_2 equal to 2×10^{-4}, and a cosmic-ray ionization rate of $3 \times 10^{-17} \, s^{-1}$, one obtains $n_H \sim 2 \, cm^{-3}$

and $R \sim 26–2.6$. That is, the H_2 formation rate dominates over the CO freezing one. Therefore, frozen CO molecules can potentially be desorbed by the energy released by the H_2 formation on the icy grain surfaces. This process, if confirmed, might naturally explain the presence of gaseous CO in not too dense ($n_H \lesssim 10^4 \, cm^{-3}$) molecular clouds and solve a decades-long mystery. However, to put this affirmation on solid ground, specific AIMDs showing the effective sublimation of the CO molecule as well as larger ASW ice models and dedicated astrochemical modeling simulations that include this effect are mandatory. They will be the focus of forthcoming works.

4.2. H_2 Vibrational State

Previous experimental and computational works on graphite surfaces show that after its formation, the H_2 molecule populates vibrational levels around $\nu = 3–4$ (Latimer et al. 2008; Islam et al. 2010; Casolo et al. 2013). On crystalline and amorphous ice surfaces only a few studies were carried out. Based on classical MD simulations, Takahashi et al. (1999a) and Takahashi & Uehara (2001) predicted that H_2 formed on amorphous ice would be vibrationally excited to $\nu = 7–8$. In contrast, in some laboratory experiments (Hornekær et al. 2003; Roser et al. 2003; Hama et al. 2012), the authors did not detect such excited states. Our new simulations confirm both findings: depending on the site where the formation occurs, H_2 can have large (up to 6) or low (1–2) ν (Table 1). For example, the case of ASW Pos1, which is the one in a cavity, shows the lowest ν. In the ISM, the vibrational state of the newly formed H_2 molecules will depend on the probability of H_2 leaving the grain surface before being "thermalized" by collisions with ice water molecules, as also found and discussed in Watanabe et al. (2010).

The vibrational state of the newly formed H_2 molecule, i.e., how much the molecule is vibrationally excited, has important consequences on two major astrophysical aspects:

(i) to help gas-phase reactions with high activation energy barriers, some of which are the starting points of the entire chemistry in molecular clouds (Agúndez et al. 2010); and

(ii) the possibility to detect newly formed H_2 with near-future James Webb Space Telescope (JWST) observations and, consequently, measure the rate of H_2 formation in molecular clouds and put constraints to theories.

5. Summary

We studied the energy dissipation of the H_2 formation reaction on both crystalline and amorphous (ASW) ice models by means of state-of-the-art ab initio molecular dynamics simulations (AIMDs). In the ASW ice, we explored three formation sites meant to represent different situations in terms of energetics and surface morphology: one is in a cavity (Pos1) and the other two are in the outermost parts of the surface (Pos2 and Pos3).

In all simulations, we found that about at least 30% of the reaction energy ($\sim 440 \, kJ \, mol^{-1}$) is acquired by the newly formed H_2, namely more than 10 times the H_2 binding energy ($\sim 10 \, kJ \, mol^{-1}$), so that H_2 is likely doomed to leave the ice and to be injected into the gas. The remaining two-thirds of the reaction energy are absorbed by the water ice in less than 1 ps. The water molecules nearby the reaction site have energy peaks

of 7–43 kJ mol^{-1} for more than 100–200 fs, while those within a 4.0 Å radius of 3–14 kJ mol^{-1}.

We showed that it is in principle possible that frozen CO molecules close to the H_2 formation site sublimate. If confirmed, this will be a simple explanation to the decades-long conundrum of why gaseous CO is present in cold molecular clouds. In order to quantify this effect, new focused AIMDs, adopting larger ASW ice models and dedicated astrochemical modeling, will be necessary.

Finally, the nascent H_2 molecules have large ($\nu = 6$) vibrational states in the first picosecond and later decay to 1–2. This high vibrational state could help reactions with an activation barrier involving H_2 to occur also in cold gas and be observable by JWST.

Appendix
Computational Details

Proper reactant spin localization is achieved by relying on the unrestricted-DFT broken (spin) symmetry approach. This is mandatory when dealing with diradical systems in singlet electronic state. In the $H + H$ specific case, despite the total spin moment on the global system being 0, the unpaired electrons on the two H atoms are expected to have spin α (i.e. $+1$) and β (i.e. -1) each.

In order to check the quality of our results, in Table A1 a comparison between the H_2 formation energy in the gas phase calculated at PBE and CCSD(T) levels is presented. Moreover, the interaction between H_2 and one H_2O molecule was also

Table A1
Adsorption and Reaction ($H + H \rightarrow H_2$) Energy Data

	Reaction Energy (kJ mol^{-1})
Crystalline	−438.9
Pos1	−436.2
Pos2	−435.9
Pos3	−440.3
H_2 CP2K[a]	−440.6
H_2 Gaussian[b]	−457.4

	Binding Energy (kJ mol^{-1})
CP2K[a]	4.1
Gaussian[b]	2.6

Notes.
[a] H_2 gas-phase reaction energy calculated at PBE-D3/TZVP level.
[b] H_2 gas-phase reaction energy calculated at CCSD(T)/aug-cc-pv5z level.

(a) Crystalline ice

(b) Amorphous ice Pos1
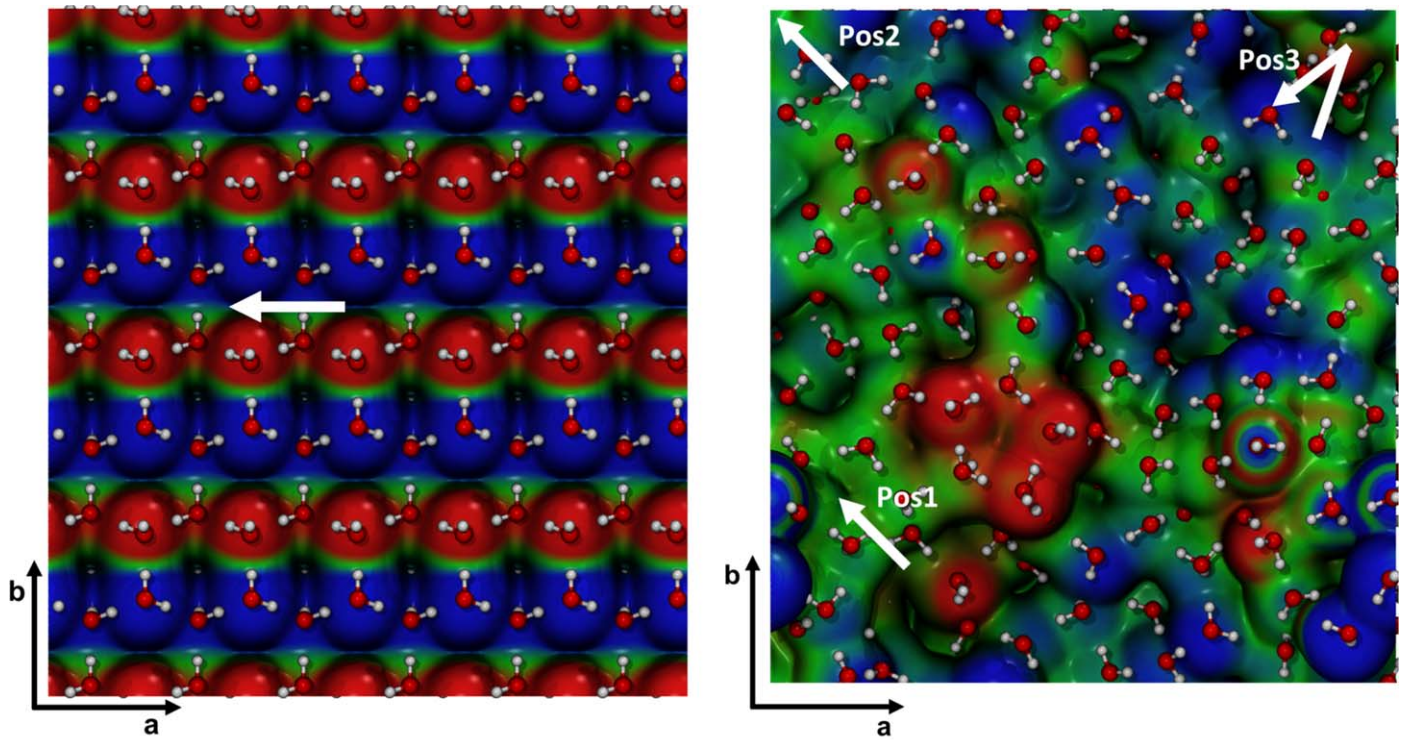
(c) Amorphous ice Pos2

(d) Amorphous ice Pos3
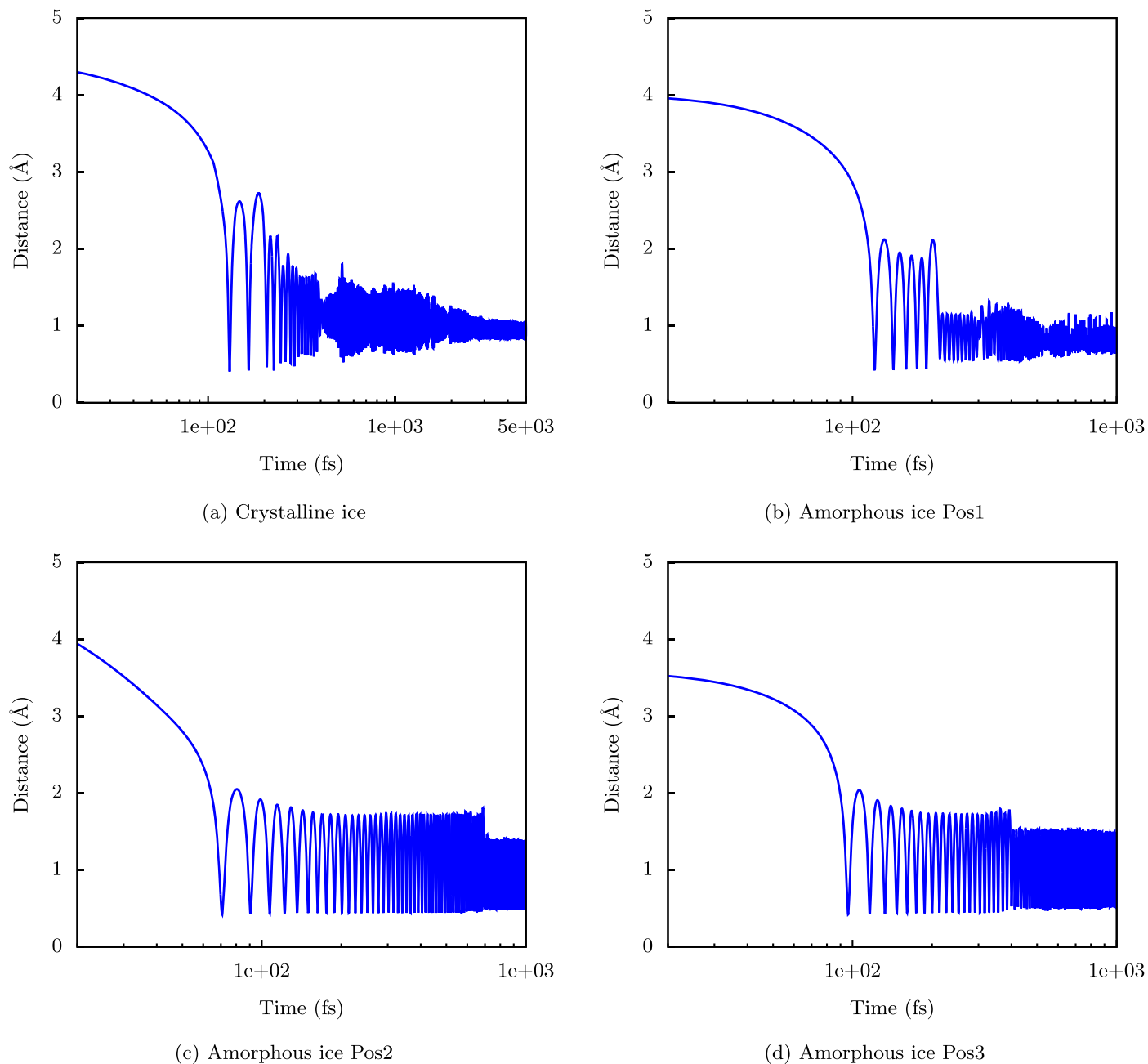
Figure A1. Evolution of the H–H bond distance during the AIMD simulations.

evaluated at the same levels of theory, giving results in good agreement. Additionally, the interaction between H_2 and one H_2O molecule was also evaluated at the same levels of theory, giving results in good agreement. The difference between the two methodologies is acceptable, considering the energy released by the reaction.

Regarding the AIMD simulations, we run an equilibration AIMD in the NVT ensemble (using the CSVR thermostat, with a time constant of 20 femtoseconds) at 10 K for 1 ps (with a time step of 1 fs) only for the bare ice surface. This ensures an initial thermally equilibrated ice. Then the velocities of the equilibrated ice surfaces are used as input for the NVE production runs. Those velocities correspond to the initial kinetic energy of the ice, as presented in Figure 3. The H velocities, instead, were manually set to favor the H–H bond formation respecting the 10 K limitation. In Figures A1–A3 the evolution of the H–H distance, the electrostatic potential map of the bare surface, and the snapshot of the adduct (H_3O^+–H^-) are reported, respectively.

(a) Crystalline ice: top view

(b) Amorphous ice: top view
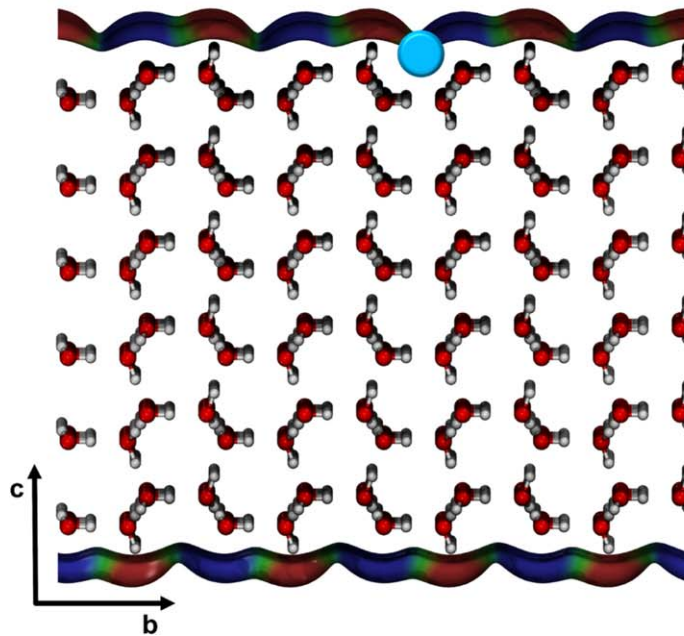
(c) Crystalline ice: lateral view

Figure A2. Top view of the electrostatic potential map of the crystalline (a) and amorphous (b) ice models. Lateral view of the crystalline ice model (c). White arrows represent the H_2 diffusion direction. The light blue circle in the bottom panel represents the cavity inside of which the H_2 diffuses over the crystalline ice model. Red and blue zones of the electrostatic maps correspond to positive and negative potentials. O atoms in red, H atoms in white.

(a) H$_2$ kinetic energy

(b) H$_2$O kinetic energy

(c) Time: 0 fs

(d) Time: 206.6 fs
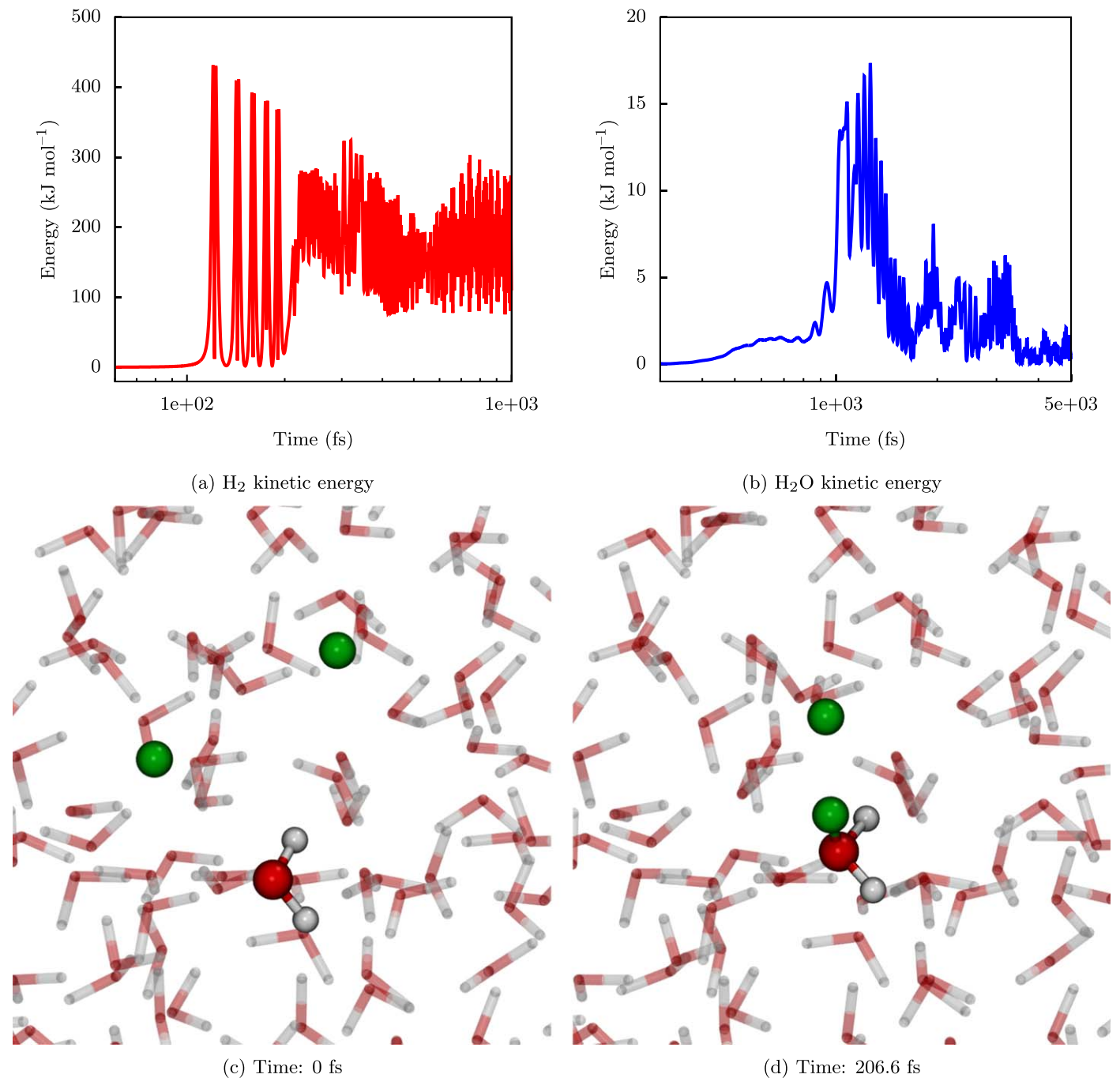
Figure A3. Evolution of the kinetic energy of H$_2$ (panel (a)) and a neighbor water molecule (panel (b)) for the amorphous Pos1 case. Starting position of the AIMD simulation (panel (c)) and formation of the H$^-$/H$_3$O$^+$ adduct after 0.2 ps of simulation (panel (d)). O atoms are in red, and H atoms are in white. The H atoms highlighted in green are the reactants.

ORCID iDs

Stefano Pantaleone ⓘ https://orcid.org/0000-0002-2457-1065
Joan Enrique-Romero ⓘ https://orcid.org/0000-0002-2147-7735
Cecilia Ceccarelli ⓘ https://orcid.org/0000-0001-9664-6292
Stefano Ferrero ⓘ https://orcid.org/0000-0001-7819-7657
Nadia Balucani ⓘ https://orcid.org/0000-0001-5121-5683
Albert Rimola ⓘ https://orcid.org/0000-0002-9637-4554
Piero Ugliengo ⓘ https://orcid.org/0000-0001-8886-9832

References

Agúndez, M., Goicoechea, J., Cernicharo, J., Faure, A., & Roueff, E. 2010, ApJ, 713, 662
Boogert, A. C. A., Gerakines, P. A., & Whittet, D. C. B. 2015, ARA&A, 53, 541
Casolo, S., Tantardini, G. F., & Martinazzo, R. 2013, PNAS, 110, 6674
Duley, W. W., & Williams, D. A. 1993, MNRAS, 260, 37
Ferrero, S., Zamirri, L., Ceccarelli, C., et al. 2020, ApJ, 904, 11
Goedecker, S., Teter, M., & Hutter, J. 1996, PhRvB, 54, 1703
Grimme, S., Antony, J., Ehrlich, S., & Krieg, H. 2010, JChPh, 132, 154104
Grimme, S., Ehrlich, S., & Goerigk, L. 2011, JCoCh, 32, 1456
Hama, T., Kuwahata, K., Watanabe, N., et al. 2012, ApJ, 757, 185

Hasegawa, T. I., & Herbst, E. 1993, MNRAS, 261, 83
He, J., Acharyya, K., & Vidali, G. 2016, ApJ, 825, 89
Herbst, E., & Cuppen, H. M. 2006, PNAS, 103, 12257
Hincelin, U., Chang, Q., & Herbst, E. 2015, A&A, 574, A24
Hollenbach, D., & Salpeter, E. 1970, JChPh, 53, 79
Hollenbach, D., & Salpeter, E. 1971, ApJ, 163, 155
Hornekær, L., Baurichter, A., Petrunin, V., Field, D., & Luntz, A. 2003, Sci, 302, 1943
Hutter, J., Iannuzzi, M., Schiffmann, F., & VandeVondele, J. 2014, WIREs Comput. Mol. Sci, 4, 15
Islam, F., Cecchi-Pestellini, C., Viti, S., & Casu, S. 2010, ApJ, 725, 1111
Ivlev, A., Röcker, T., Vasyunin, A., & Caselli, P. 2015, ApJ, 805, 59
Jorgensen, W. L., Chandrasekhar, J., Madura, J. D., Impey, R. W., & Klein, M. L. 1983, JChPh, 79, 926
Latimer, E. R., Islam, F., & Price, S. D. 2008, CPL, 455, 174
Léger, A. 1983, A&A, 123, 271
Leger, A., Jura, M., & Omont, A. 1985, A&A, 144, 147
Lippert, G., Hutter, J., & Parrinello, M. 1997, MolPh, 92, 477
Molpeceres, G., & Kästner, J. 2020, PCCP, 22, 7552
Pantaleone, S., Enrique-Romero, J., Ceccarelli, C., et al. 2020, ApJ, 897, 56

Perdew, J., Burke, K., & Ernzerhof, M. 1996, PhRvL, 77, 3865
Roser, J., Swords, S., Vidali, G., Manico, G., & Pirronello, V. 2003, ApJL, 596, L55
Ruocco, G., Sette, F., Bergmann, U., et al. 1996, Natur, 379, 521
Schutte, W., & Greenberg, J. 1991, A&A, 244, 190
Shen, C., Greenberg, J., Schutte, W., & Van Dishoeck, E. 2004, A&A, 415, 203
Smith, R. G., Sellgren, K., & Tokunaga, A. T. 1988, ApJ, 334, 209
Smoluchowski, R. 1983, JPhCh, 87, 4229
Takahashi, J. 1999, EP&S, 51, 1215
Takahashi, J., Masuda, K., & Nagaoka, M. 1999a, ApJ, 520, 724
Takahashi, J., Masuda, K., & Nagaoka, M. 1999b, MNRAS, 306, 22
Takahashi, J., & Uehara, H. 2001, ApJ, 561, 843
Takahashi, J., & Williams, D. A. 2000, MNRAS, 314, 273
van de Hulst, H. C. 1946, RAOU, 11, 2
Vidali, G. 2013, ChRv, 113, 8762
Wakelam, V., Bron, E., Cazaux, S., et al. 2017, MolAs, 9, 1
Watanabe, N., Kimura, Y., Kouchi, A., et al. 2010, ApJL, 714, L233
Whittet, D. C. B. 1993, in Dust and Chemistry in Astronomy, ed. T. J. Millar & D. A. Williams (Boca Raton, FL: Routledge), 9